




## Hall bar measurements of topological surface states of (001) cadmium arsenide thin films interfaced with superconductors

Binghao Guo , Alexander C. Lygo, Tyler N. Pardue, and Susanne Stemmer <sup>\*</sup>  
*Materials Department, University of California, Santa Barbara, California 93106-5050, USA*

 (Received 10 December 2021; revised 30 January 2022; accepted 7 March 2022; published 16 March 2022)

Hybrid structures consisting of a topological insulator brought in proximity to an *s*-wave superconductor are one of the most promising routes to topological superconductivity and Majorana quasiparticles. A key challenge is the superconductor/topological insulator interface, which must be transparent to Cooper pairs while also preserving high-mobility topological states. Here, we investigate Hall bar devices fabricated on the topological insulator-like surfaces of (001) cadmium arsenide films, which we partially cover with different superconductors. We show that, depending on the magnitude of a perpendicular magnetic field, devices with sputter-deposited Nb exhibit superconductivity and the quantum Hall effect from the topological surface states, respectively. By contrast, devices with thermally evaporated Sn do not show superconductivity, indicating poor interface transparency. We discuss the coupling between the superconductor and the surface states.

DOI: [10.1103/PhysRevMaterials.6.034203](https://doi.org/10.1103/PhysRevMaterials.6.034203)

### I. INTRODUCTION

Topological superconductors have a superconducting energy gap in the bulk and gapless quasiparticle states at their boundaries or at defects [1]. Experimental searches for these quasiparticles are driven by their potential application as robust qubits in quantum computing algorithms [2] as well as basic scientific interest. Besides intrinsic candidate compounds, a topological superconductor can also be engineered at interfaces in hybrid structures [3]. One of the most prominent approaches is based on a theoretical proposal by Fu and Kane [4], which involves interfacing an *s*-wave superconductor with the surface (or edge) states of a topological insulator. The practical realization of the Fu-Kane proposal requires a number of variables that need to be understood together, such as the role of various material properties and their compatibility at the interface. While hybrid structures with topological insulators are believed to be less sensitive to disorder than other approaches [5], interfaces must nevertheless preserve the topological boundary states, and, at the same time, they must be transparent to the Cooper pairs. For example, Ar plasma treatments are generally employed to improve the transparency of the interface [6,7], but highly energetic processes may cause structural damage even deep below the surface, as is well known from semiconductor processing [8]. Hence, interpreting transport signatures of hybrid superconductor/topological devices can be challenging [9] and requires a thorough understanding of the properties of the topological surface states *after* they have been interfaced with a particular superconductor.

Recently, epitaxial films of the topological semimetal cadmium arsenide ( $\text{Cd}_3\text{As}_2$ ) have attracted attention for their tunability. Unlike bulk  $\text{Cd}_3\text{As}_2$ , which is a three-dimensional Dirac semimetal [10], (001) thin films feature a gapped bulk

while the top and bottom surfaces each host a single Dirac fermion [11–13], just like in a three-dimensional topological insulator. The bulk band gap and the mobility of the surface states are large, as evidenced, for example, by observations of the quantum Hall effect from the surface states without interference from bulk carriers [11–13]. This makes (001)  $\text{Cd}_3\text{As}_2$  a promising platform to realize the Fu-Kane proposal. While induced superconductivity has been investigated for (112) surfaces of  $\text{Cd}_3\text{As}_2$  [14–16], these samples were bulklike and thus not suitable for realizing proposals that involve inducing superconductivity into the surface states of a topological insulator.

The goal of the present study is to evaluate the influence of depositing different *s*-wave superconductors on the topological surface states of cadmium arsenide. To this end, we investigate Hall bars that have a superconducting strip covering the center region of the device mesa. Optical micrographs and a device schematic are shown in Fig. 1. One of the devices uses Sn, a type-I superconductor that is thermally evaporated. The other Hall bar is covered with Nb, a type-II superconductor that is sputtered due to its high melting point, which is a more damaging metallization process than thermal evaporation [8]. The Nb devices exhibit both superconductivity and the quantum Hall effect from the surface states. In the case of Sn, the topological surface states are preserved, but superconductivity is not detected, despite the fact that Sn is superconducting. We discuss the origin of the differences between these devices and the implications for the application of these interfaces in topological superconducting hybrid structures.

### II. EXPERIMENT

A 20-nm-thin, (001)-oriented  $\text{Cd}_3\text{As}_2$  film was grown on (001) GaSb substrates by molecular beam epitaxy, following the steps described in Ref. [17]. An  $\text{Al}_{0.5}\text{In}_{0.5}\text{Sb}$  alloy, which has a lattice parameter that closely matches the pseudocubic lattice spacing of  $\text{Cd}_3\text{As}_2$ , served as the buffer layer between

<sup>\*</sup>stemmer@mrl.ucsb.edu

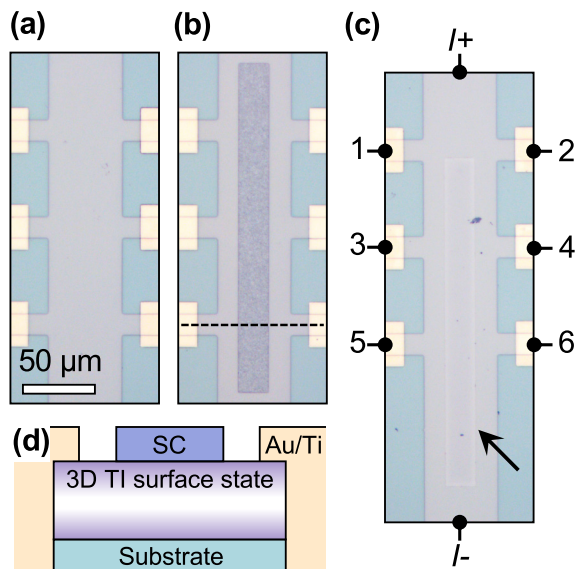


FIG. 1. Optical micrographs of (a) control device, (b) partially Sn-covered device, and (c) partially Nb-covered device. Nb is transparent and more difficult to make out than Sn, which is granular. The arrow in panel (c) points to the outline of the Nb region. The Nb strip does not cover the region between contacts 1 and 2. Voltage contacts of the Nb-covered device are labeled. The Sn and Nb regions both measure  $20\mu\text{m} \times 220\mu\text{m}$  with a nominal thickness of 30 nm. (d) Cross-sectional schematic along the dashed line in panel (b). Dimensions in the schematic are not to scale.

the  $\text{Cd}_3\text{As}_2$  film and the substrate. The surface of the  $\text{Cd}_3\text{As}_2$  film was capped *in situ* by a 3-nm-thin GaSb layer to protect it from exposure to ambient conditions while also reducing the number of device processing steps required [18]. Details regarding the low-temperature growth of GaSb are provided in the Supplemental Material [19]. All results reported here are from devices fabricated from the same wafer, unless stated otherwise. After growth,  $50\mu\text{m} \times 50\mu\text{m}$  Hall bars were patterned by photolithography, mesa isolated by Ar ion beam etching, and contacted by sputtered Au/Ti leads. Two separate processes were then used for depositing the superconductor in the center of the Hall bar (see Fig. 1), which were also patterned by liftoff. Sn (99.9999% Alfa Aesar) was thermally evaporated with rates between 1 and 5  $\text{\AA}/\text{s}$  in a custom chamber with a base pressure of less than  $3 \times 10^{-6}$  Torr. Magnetron sputtering at a DC power of 250 W was used for Nb deposition (99.95% Angstrom Sciences Inc.) under 30 standard cubic centimeters per minute of Ar gas flow at a chamber pressure of 4 mTorr. Electrical measurements were carried out in a Quantum Design Physical Property Measurement System Dynacool in magnetic fields ( $B$ ) up to 9 T. Longitudinal resistances ( $R_{xx}$ ) were symmetrized and Hall resistances ( $R_{xy}$ ) were antisymmetrized with respect to the direction of  $B$ . The superconducting transition temperature ( $T_C$ ) of a 30-nm Sn film deposited on  $\text{Cd}_3\text{As}_2$  was 3.6 K, which is close to bulk Sn, as determined from a separate sample (see Supplemental Material [19]). The superconducting properties of the Hall bars with Nb are discussed below. Cross-section transmission electron microscopy studies of the devices (see details in the Supplemental Material [19]) showed that the Nb film was

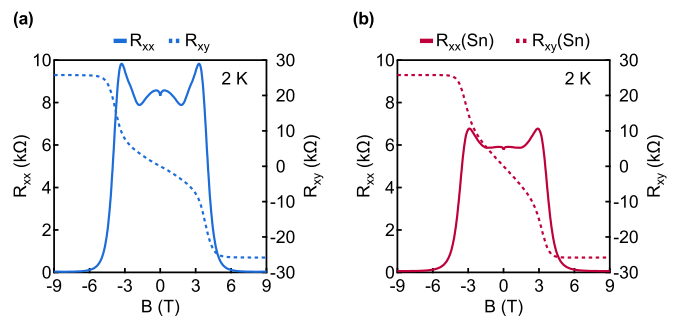


FIG. 2. Longitudinal and Hall resistances of (a) control device and (b) partially Sn-covered device at 2 K. The measurement setup for both devices was  $R_{xy} = V_{1,2}/I_{\text{bias}}$  and  $R_{xx} = V_{4,6}/I_{\text{bias}}$ .

continuous and uniform. In contrast, the Sn film was granular and did not fully cover all of the  $\text{Cd}_3\text{As}_2$  film's surface (see Supplemental Material [19]), despite being superconducting. This shows poor wetting behavior of thermally evaporated Sn on  $\text{Cd}_3\text{As}_2$ . No reaction layers could be detected at either interface [19]; any differences between the devices, discussed below, are therefore not caused by the presence of a reaction product at the interface.

Optical micrographs of three Hall bar devices are shown in Fig. 1. Figure 1(a) depicts the pristine (i.e., not covered by a superconductor) control device, a standard eight-terminal Hall bar. On the other devices a strip of Sn (or Nb) is centered on the Hall bar mesa, leaving a  $15\text{-}\mu\text{m}$ -wide gap from the mesa periphery. The distances between the superconductor and the neighboring voltage measurement contacts are at least  $27.5\mu\text{m}$ . The partially Nb-covered device further differs from the Sn one by having its superconducting strip offset to create a pristine region between the contacts labeled 1 and 2 [see Fig. 1(c)]. A cross-sectional schematic of the devices is provided in Fig. 1(d).

### III. RESULTS AND DISCUSSION

We first compare the magnetotransport results of the Sn-covered device against the control device. Figure 2 shows  $R_{xx}$  and  $R_{xy}$  of the control and Sn devices, respectively, measured at 2 K. The measurement setup for both devices was  $R_{xy} = V_{1,2}/I_{\text{bias}}$  and  $R_{xx} = V_{4,6}/I_{\text{bias}}$ , where the voltage subscripts refer to contacts as indicated in Fig. 1(c). At low magnetic fields ( $|B| < 0.5$  T), we extract a Hall mobility,  $\mu_H$ , of  $2190\text{ cm}^2\text{ V}^{-1}\text{ s}^{-1}$  and a carrier density,  $n_{2D}$ , of  $3.42 \times 10^{11}\text{ cm}^{-2}$  for the control device. The corresponding values for the Sn-covered device are  $\mu_H = 6122\text{ cm}^2\text{ V}^{-1}\text{ s}^{-1}$  and  $n_{2D} = 1.76 \times 10^{11}\text{ cm}^{-2}$ . The nearly threefold larger  $\mu_H$  for the Sn-covered device can be attributed to the lower  $n_{2D}$  of this sample (in Dirac materials, the Hall mobility is inversely proportional to the carrier density [20]). Despite the differences in carrier density and mobility, the quantum transport properties of the two devices are remarkably similar. Around  $B = 4$  T, both devices develop a clear  $\nu = 1$  quantum Hall plateau in  $R_{xy}$  that is accompanied by near-zero  $R_{xx}$ . The difference in  $n_{2D}$  is reflected in the small difference in the onset of the quantum Hall plateau. The quantum Hall effect is caused by the topological insulator-like surface states of the thin  $\text{Cd}_3\text{As}_2$

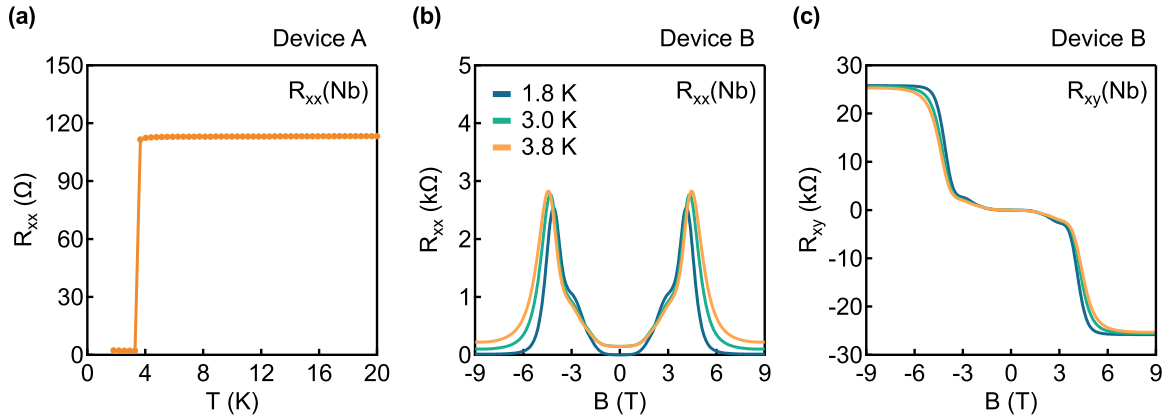


FIG. 3. Temperature and field dependence of two partially Nb-covered devices. (a) Longitudinal resistance of device A as a function of temperature. A superconducting transition appears near 3.6 K. (b) Longitudinal and (c) Hall resistances of device B at 1.8, 3.0, and 3.8 K. The measurement setup for both Nb-covered devices was  $R_{xy} = V_{3,4}/I_{\text{bias}}$  and  $R_{xx} = V_{4,6}/I_{\text{bias}}$ .

film, as discussed in detail elsewhere [11,12]. Both devices also show weak antilocalization (WAL), typical of transport in topological surface states [21,22]. We therefore conclude that thermal evaporation of Sn on the  $\text{Cd}_3\text{As}_2$  mesa does not impact the topological surface states. Transport in this device is dominated by the  $\text{Cd}_3\text{As}_2$  surface states. In particular, besides WAL, there is no superconductivity in the Hall bar devices, even though the Sn film itself becomes superconducting (additional measurements with more data points at fields below the critical field of Sn are shown in the Supplemental Material [19]). This is in contrast to the devices with Nb, which we will discuss next.

Figure 3(a) shows  $R_{xx}$  of one of the Nb-covered Hall bar devices (device A) as a function of temperature at zero magnetic field. The contact configuration was  $R_{xx} = V_{4,6}/I_{\text{bias}}$ . The temperature dependence of  $R_{xx}$  clearly shows the superconducting transition of Nb. In particular,  $R_{xx}$  drops by more than a factor of 100 as the temperature is reduced below 3.6 K, consistent with a transition to a superconducting state and current flow through the Nb. Figures 3(b) and 3(c) show the magnetic field dependence of  $R_{xx}$  and  $R_{xy}$  measured on device B at three different temperatures. Here,  $R_{xx} = V_{4,6}/I_{\text{bias}}$  and  $R_{xy} = V_{3,4}/I_{\text{bias}}$ . The main difference, relative to the control device shown in Fig. 2(a), is at low  $B$ , where  $R_{xx}$  vanishes and  $R_{xy}$  shows a much weaker  $B$  dependence, consistent with superconductivity. As expected from the temperature dependence shown in Fig. 3(a), the  $R_{xx}$  trace taken at 1.8 K, i.e., below  $T_c$  ( $\sim 3.6$  K) has lower resistance values near  $B = 0$  than the two traces recorded at 3.0 and 3.8 K, respectively. Above the critical field of Nb, the Hall coefficient remains small, as  $R_{xy}$  varies slowly at low  $B$ , reflecting an increased carrier density relative to the control device, consistent with carrier transport through the Nb even in the nonsuperconducting state. At 3.8 K (above  $T_c$ ), for example,  $n_{2D} = 7.9 \times 10^{12} \text{ cm}^{-2}$ , which is more than an order of magnitude higher than the control device. The Nb contribution is also evidenced by a monotonic increase of  $R_{xx}$  with increasing field. Thus, current flows through the Nb until the sample reaches a well-developed Hall plateau. In particular, at  $B > 3$  T, both  $R_{xx}$  and  $R_{xy}$  resemble those of the control device, exhibiting a clearly developed  $\nu = 1$  plateau in  $R_{xy}$  and the associated peak in  $R_{xx}$  at 4.5 T. We also note that

the shoulder on the low-field side of the main  $R_{xx}$  peak is also present in the control device, though it is less well resolved there, indicating a small difference in the detuning of the top and bottom surfaces between the devices (the interpretation of the details of the quantum oscillations in terms of the two sets of surface states of a topological insulator is discussed in detail elsewhere [11,12]). The important conclusion for this study is that at low fields, the presence of the Nb layer significantly changes the transport characteristics of the device, in contrast to Sn. At high fields, however, we see only the quantum Hall effect from the surface states and transport is similar to the control device.

We interpret the results from the Nb-covered devices in terms of two transport regimes of the surface states. At low  $B$ , the Landau quantization of the surface states is not fully developed (the sample is not yet in the quantum Hall regime) and therefore the two-dimensional bulk of the surface is not insulating. The bulk of the not yet quantized surface serves as a contact to the Nb-covered region of the device. Within the quantum Hall plateau, the two-dimensional bulk of the surface is insulating, and charge transport occurs only through the edge channel(s). As a result, the Nb-covered region is effectively isolated (any edge channels around the Nb island are not contacted) and no current flows through the Nb. This interpretation is confirmed also by the behavior of the devices at higher temperatures (10 K) [19].

It is important to note that our measurements cannot distinguish between proximity-induced superconductivity in the  $\text{Cd}_3\text{As}_2$  surface vs superconductivity in the Nb itself. Evidence for proximitized superconductivity and its nature requires other measurements, i.e., of Josephson effects, which are beyond the scope of this work. Independent of the question of induced superconductivity, however, the fact that we detect superconductivity in the Nb-covered devices indicates good interface transparency, while, at the same time, the intrinsic transport properties of the topological surface states are preserved. In particular, the observation of the quantum Hall effect at relatively modest fields is clear evidence for the presence of high-mobility surface states. Both are necessary conditions for the realization of topological superconductivity in hybrid structures.

It is instructive to compare the Nb-covered devices to those covered by Sn, which also becomes superconducting. These devices do not show superconductivity or transport through the thermally evaporated Sn. Instead, transport is dominated by the surface states at all fields; for example, WAL indicates transport through the surface states, including below the critical field of Sn.

Collectively, these results show that the interface with Sn is not as transparent as the interface with Nb. The reduced  $n_{2D}$  after Sn deposition is consistent with the formation of a barrier that results in carrier depletion. In general, surface treatment and/or overlayers have a significant influence on surface band bending in  $\text{Cd}_3\text{As}_2$  [18]. The observed poor wetting behavior of Sn on the capped  $\text{Cd}_3\text{As}_2$  surface is an indicator that good electrical contact between these two materials is more difficult to establish than for the Nb interface. In addition, sputtering, which is more energetic than thermal deposition, may also serve to provide a better electrical contact, for example by removing surface adsorbates or causing a small degree of intermixing that is not detectable in the electron micrographs. It is therefore possible that better coupling between Sn and  $\text{Cd}_3\text{As}_2$  could be achieved by modifying the deposition process.

#### IV. CONCLUSIONS

To summarize, we have studied a simple device structure that allows for determining the quality of hybrid interfaces,

which are needed to realize different proposals of topological superconductivity. The devices allow for determining interface transparency for different superconductor/topological insulator combinations. For example, our results show that sputtered Nb/(001)  $\text{Cd}_3\text{As}_2$  interfaces are potentially suitable as a platform for realizing the Fu-Kane proposal, as the devices exhibit superconductivity and the quantum Hall effect from the topological surface states. The latter feature shows that  $\text{Cd}_3\text{As}_2$  may also be of interest to more recent proposals for non-Abelian quasiparticles, which involve inducing superconductivity into quantum Hall edge states [23–25]. Such devices will require a superconductor with a higher critical field than Nb.

#### ACKNOWLEDGMENTS

The authors thank Dr. David Kealhofer for helpful discussions. The work was supported by the Office of Naval Research (Grant No. N00014-21-1-2474). B.G. thanks the UCSB Quantum Foundry for support, which is funded via the Q-AMASE-i program of the U.S. National Science Foundation (NSF) under Award Grant No. DMR-1906325. A.C.L. and T.N.P. thank the U.S. National Science Foundation Graduate Research Fellowship Program for support (Grant No. 1650114). This work made use of the MRL Shared Experimental Facilities, which are supported by the MRSEC Program of the U.S. National Science Foundation under Award No. DMR 1720256.

- 
- [1] X. L. Qi and S. C. Zhang, Topological insulators and superconductors, *Rev. Mod. Phys.* **83**, 1057 (2011).
  - [2] A. Y. Kitaev, Fault-tolerant quantum computation by anyons, *Ann. Phys.* **303**, 2 (2003).
  - [3] J. Alicea, New directions in the pursuit of Majorana fermions in solid state systems, *Rep. Prog. Phys.* **75**, 076501 (2012).
  - [4] L. Fu and C. L. Kane, Superconducting Proximity Effect and Majorana Fermions at the Surface of a Topological Insulator, *Phys. Rev. Lett.* **100**, 096407 (2008).
  - [5] A. C. Potter and P. A. Lee, Engineering a  $p + i p$  superconductor: Comparison of topological insulator and Rashba spin-orbit-coupled materials, *Phys. Rev. B* **83**, 184520 (2011).
  - [6] C. Nguyen, H. Kroemer, and E. L. Hu, Contact resistance of superconductor-semiconductor interfaces: The case of Nb-InAs/AlSb quantum-well structures, *Appl. Phys. Lett.* **65**, 103 (1994).
  - [7] L. Maier, J. B. Oostinga, D. Knott, C. Brüne, P. Virtanen, G. Tkachov, E. M. Hankiewicz, C. Gould, H. Buhmann, and L. W. Molenkamp, Induced Superconductivity in the Three-Dimensional Topological Insulator HgTe, *Phys. Rev. Lett.* **109**, 186806 (2012).
  - [8] C. H. Chen, E. L. Hu, W. V. Schoenfeld, and P. M. Petroff, Metallization-induced damage in III-V semiconductors, *J. Vac. Sci. Technol. B* **16**, 3354 (1998).
  - [9] S. M. Frolov, M. J. Manfra, and J. D. Sau, Topological superconductivity in hybrid devices, *Nat. Phys.* **16**, 718 (2020).
  - [10] Z. J. Wang, H. M. Weng, Q. S. Wu, X. Dai, and Z. Fang, Three-dimensional Dirac semimetal and quantum transport in  $\text{Cd}_3\text{As}_2$ , *Phys. Rev. B* **88**, 125427 (2013).
  - [11] D. A. Kealhofer, L. Galletti, T. Schumann, A. Suslov, and S. Stemmer, Topological Insulator State and Collapse of the Quantum Hall Effect in a Three-Dimensional Dirac Semimetal Heterojunction, *Phys. Rev. X* **10**, 011050 (2020).
  - [12] D. A. Kealhofer, M. Goyal, T. N. Pardue, and S. Stemmer, Thickness-independent transport in thin (001)-oriented cadmium arsenide films, *Phys. Rev. B* **104**, 035435 (2021).
  - [13] L. Galletti, A. Rashidi, D. A. Kealhofer, M. Goyal, B. H. Guo, Y. T. Li, C. Shang, J. E. Bowers, and S. Stemmer, Quantum Hall effect of the topological insulator state of cadmium arsenide in Corbino geometry, *Appl. Phys. Lett.* **118**, 261901 (2021).
  - [14] C. Z. Li, C. Li, L. X. Wang, S. Wang, Z. M. Liao, A. Brinkman, and D. P. Yu, Bulk and surface states carried supercurrent in ballistic Nb-Dirac semimetal  $\text{Cd}_3\text{As}_2$  nanowire-Nb junctions, *Phys. Rev. B* **97**, 115446 (2018).
  - [15] W. Yu, W. Pan, D. L. Medlin, M. A. Rodriguez, S. R. Lee, Z. Q. Bao, and F. Zhang,  $\pi$  and  $4\pi$  Josephson Effects Mediated by a Dirac Semimetal, *Phys. Rev. Lett.* **120**, 177704 (2018).
  - [16] C. Huang, B. T. Zhou, H. Q. Zhang, B. J. Yang, R. Liu, H. W. Wang, Y. M. Wan, K. Huang, Z. M. Liao, E. Z. Zhang, S. S. Liu, Q. S. Deng, Y. H. Chen, X. D. Han, J. Zou, X. Lin, Z. Han,

- Y. H. Wang, K. T. Law, and F. X. Xiu, Proximity-induced surface superconductivity in Dirac semimetal  $\text{Cd}_3\text{As}_2$ , *Nat. Commun.* **10**, 2217 (2019).
- [17] M. Goyal, S. Salmani-Rezaie, T. N. Pardue, B. H. Guo, D. A. Kealhofer, and S. Stemmer, Carrier mobilities of (001) cadmium arsenide films, *APL Mater.* **8**, 051106 (2020).
- [18] L. Galletti, T. Schumann, T. E. Mates, and S. Stemmer, Nitrogen surface passivation of the Dirac semimetal  $\text{Cd}_3\text{As}_2$ , *Phys. Rev. Mater.* **2**, 124202 (2018).
- [19] See Supplemental Material at <http://link.aps.org/supplemental/10.1103/PhysRevMaterials.6.034203> for a description of the growth of the GaSb cap layer, atomic force microscopy images of the surfaces, the superconducting properties of Sn on  $\text{Cd}_3\text{As}_2$ , transmission electron microscopy images, quantum Hall effect measurements to higher temperatures, and a low-field scan of the Sn-covered Hall bar.
- [20] E. H. Hwang, S. Adam, and S. Das Sarma, Carrier Transport in Two-Dimensional Graphene Layers, *Phys. Rev. Lett.* **98**, 186806 (2007).
- [21] A. A. Taskin, S. Sasaki, K. Segawa, and Y. Ando, Manifestation of Topological Protection in Transport Properties of Epitaxial  $\text{Bi}_2\text{Se}_3$  Thin Films, *Phys. Rev. Lett.* **109**, 066803 (2012).
- [22] O. F. Shoron, D. A. Kealhofer, M. Goyal, T. Schumann, A. A. Burkov, and S. Stemmer, Detecting topological phase transitions in cadmium arsenide films via the transverse magnetoresistance, *Appl. Phys. Lett.* **119**, 171907 (2021).
- [23] Z. Wan, A. Kazakov, M. J. Manfra, L. N. Pfeiffer, K. W. West, and L. P. Rokhinson, Induced superconductivity in high-mobility two-dimensional electron gas in gallium arsenide heterostructures, *Nat. Commun.* **6**, 7426 (2015).
- [24] F. Amet, C. T. Ke, I. V. Borzenets, J. Wang, K. Watanabe, T. Taniguchi, R. S. Deacon, M. Yamamoto, Y. Bomze, S. Tarucha, and G. Finkelstein, Supercurrent in the quantum Hall regime, *Science* **352**, 966 (2016).
- [25] G. H. Lee, K. F. Huang, D. K. Efetov, D. S. Wei, S. Hart, T. Taniguchi, K. Watanabe, A. Yacoby, and P. Kim, Inducing superconducting correlation in quantum Hall edge states, *Nat. Phys.* **13**, 693 (2017).